# Demonstration of broad photonic crystal stop band in a freely-suspended microfiber perforated by an array of rectangular holes

**Yang Yu,[1,3] Wei Ding,[1,*] Lin Gan,[1] Qiang Luo,[2] Steve Andrews,[4] and Zhi-Yuan Li[1]**

[1]*Laboratory of Optical Physics, Institute of Physics, Chinese Academy of Sciences, Beijing 100190, China*
[2]*International Center for Quantum Materials, Peking University, Beijing 100871, China*
[3]*School of Physics, Nankai University, Tianjin 300071, China*
[4]*Department of Physics, University of Bath, Bath BA2 7AY, United Kingdom*
*wding@iphy.ac.cn

**Abstract:** It is shown that photonic crystal (PhC) optical reflectors with reflectance in excess of 60% and fractional bandwidths greater than 10% can be fabricated by ion beam milling of fewer than ten periods of rectangular cross section through-holes in micron-scale tapered fibers. The optical characteristics agree well with numerical simulations when allowance is made for fabrication artifacts and we show that the radiation loss, which is partly determined by optical interference, can be suppressed by design. The freely-suspended devices are compact and robust and could form the basic building block of optical cavities and filters.



**OCIS codes:** (060.4005) Microstructured fibers, (220.4241) Nanostructure fabrication, (350.4238) Nanophotonics and photonic crystals.

## References and links

1. P. St. J. Russell, J. –L. Archambault, and L. Reekie, "Fibre gratings," Physics World **6**, 41 (1993).
2. M. Gnan, S. Thoms, D. S. Macintyre, R. M. De La Rue, and M. Sorel, "Fabrication of low-loss photonic wires in silicon-on-insulator using hydrogen silsesquioxane," Electron. Lett. **44**, 115 (2008).
3. J. S. Foresi, P. R. Villeneuve, J. Ferrera, E. R. Thoen, G. Steinmeyer, S. Fan, J. D. Joannopoulos, L. C. Kimerling, H. I. Smith, and E. P. Ippen, "Photonic-bandgap microcavities in optical waveguides," Nature **390**, 143 (1997).
4. K. O. Hill, Y. Fujii, D. C. Johnson, and B. S. Kawasaki, "Photosensitivity in optical fiber waveguides: Application to reflection filter fabrication," Appl. Phys. Lett. **32**, 647 (1978).
5. J. –L. Archambault, L. Reekie, and P. St. J. Russell, "100% reflectivity Bragg reflectors produced in optical fibres by single excimer laser pulses," Electron. Lett. **29**, 453 (1993).
6. W. Ding, S. R. Andrews, and S. A. Maier, "Surface corrugation Bragg gratings on optical fiber tapers created via plasma etch postprocessing," Opt. Lett. **32**, 2499 (2007).
7. Y. X. Liu, C Meng, A. P. Zhang, Y. Xiao, H. K. Yu, and L. M. Tong, "Compact microfiber Bragg gratings with high-index contrast," Opt. Lett. **36**, 3115 (2011).
8. K. P. Nayak, F. L. Kien, Y. Kawai, K. Hakuta, K. Nakajima, H. T. Miyazaki, and Y. Sugimoto, "Cavity formation on an optical nanofiber using focused ion beam milling technique," Opt. Express **19**, 14040 (2011).
9. M. Ding, M. N. Zervas, and G. Brambilla, "A compact broadband microfiber Bragg grating," Opt. Express **19**, 15621 (2011).
10. J. D. Love, W. M. Henry, W. J. Stewart, R. J. Black, S. Lacroix, and F. Gonthier, "Tapered single-mode fibres and devices Part 1: Adiabaticity criteria," IEE Proceedings-J **138**, 343 (1991).
11. A. W. Snyder and J. D. Love, *Optical Waveguide Theory*, (Chapman and Hall, London, 1983).
12. T. Erdogan, "Fiber grating spectra," J. Lightwave Technol. **15**, 1277 (1997).
13. J. D. Joannopoulos, S. G. Johnson, J. N. Winn, and R. D. Meade, *Photonic Crystals: Molding the flow of light, 2nd Edition*, (Princeton University Press, Princeton, 2008).

14. M. Gnan, G. Bellanca, H. M. H. Chong, P. Bassi, and R. M. De La Rue, "Modelling of photonic wire Bragg gratings," Opt. Quantum Electronics **38**, 133 (2006).
15. W. Ding, R. J. Liu, and Z. Y. Li, "Reducing radiation losses of one-dimensional photonic-crystal reflectors on a silica waveguide," Opt. Express **20**, 28641 (2012).

## 1. Introduction

Silica optical fibers are without doubt the most important type of optical waveguide by virtue of their excellent transparency, ease of functionalization by microstructuring or doping, and straightforward, low loss integration [1]. In the emerging area of nanophotonics microfiber devices such as high Q, small mode volume cavities, created by tapering and structuring of conventional fibers, are potentially important tools because the low refractive index of silica leads to a substantial evanescent field outside the waveguide and they are freely positionable, thus allowing stronger interaction with and more flexible access to micro- or nano-scale optical components and materials outside the waveguide. In comparison, high index semiconductor-based optical waveguides such as silicon wires are not easily reconfigurable because they have to be attached to a supporting substrate and need additional coupling optics. In addition they have weak evanescent fields and usually exhibit much higher propagation loss due to material absorption and sidewall roughness [2]. Despite such disadvantages, nearly all nano-photonic devices have so far been based on semiconductor platforms. This can be partly ascribed to the easy creation of high Q, small volume cavities in high-index waveguides as a result of the large index difference between semiconductor and air. It is recognized that such cavities are a prerequisite for enhanced light-matter interactions and high-density photonic integration. As an example, a broadband Fabry-Perot cavity in a silicon wire formed by periodic removal of material [3] only requires a few silicon-air periods to make each mirror [we call this basic building block a photonic crystal (PhC) reflector] so that the cavity length can be very short. In contrast, to do the same in a conventional germanium-doped silica fiber Bragg grating (FBG) requires hundreds of periods [4, 5], the effective cavity is thus much longer due to the substantial field penetration into the mirrors, and the bandwidth is small. This is simply because of the low index contrast in the silica-doped silica system.

Employing microfiber, which can be precisely tapered down from a conventional fiber, and then manufacturing structures by etching away selected portions seems like a good solution to improve the refractive index contrast in a fiber-based approach. Plasma etched corrugations were first made and tested on the surface of 10 μm thick microfibers [6] but strong PhC effects in this simple prototype reflector, were not observed. Later, Liu et al [7] and Nayak et al [8] adopted the more versatile focused ion beam (FIB) milling technique to make PhC reflectors in microfibers. In Liu et al's work, shallow gratings were used but the fractional reflection bandwidth was less than 0.3%. Nayak et al pushed this value to ~2% by creating deeply-indented recesses on both sides of a sub-wavelength fiber. However, both these groups restricted the depth of the etched structures to retain mechanical strength. In order to further raise the index contrast, drilling air holes into the central region of the microfiber, where the field of the guided wave is highest, is a possible way forward, as demonstrated by Ding et al [9] who created a PhC reflector with a reflection bandwidth of ~10% by milling an array of biconvex cross-section air-holes in a 1.34 μm diameter fiber. However, in the latter work a substrate was required for mechanical support which so that applications are very limited compared with a freely suspended fiber. The contact of the microfiber with the supporting material also causes serious light leakage, which greatly degrades the spectral performance.

In order to resolve the conflicting requirements of high index contrast and mechanical strength, in this letter, we report work on a slightly bigger diameter (1.7 μm) microfiber with a PhC reflector made using rectangular through-holes and find that a broad reflection bandwidth (~20%) and robust freely-suspended operation can be combined. The symmetrical shape of our etched holes prohibits energy coupling to odd-parity modes and requires us to adopt

single-even-mode rather than conventional single-mode condition, which we show is an advantage in that larger diameter fibers can be used. We also measure the radiation losses in the centre of the stop band of such a PhC reflector and show that the variation with the number of periods can be explained as an interferometric process which could be exploited to lower the total radiation loss by careful choice of the number of periods.

## 2. Device designs

Figure 1 plots the wave vector diagrams of periodic quarter-wave stacks consisting of silicon/air [Fig. 1(a)], silica/air [Fig. 1(b)], and silica/germanosilicate [Fig. 1(c)]. The central wavelengths of their stop bands and the refractive index difference between silica and germanosilicate are 1.55 μm and 0.01 respectively. A transfer matrix method was employed to calculate the real and imaginary (α) parts of the wave vector (k) of the Floquet-Bloch wave as a function of the vacuum wavelength ($\lambda_0$). From Fig. 1, it is seen that the peak value of $\alpha\Lambda$ and the width of the stop band in the silicon/air stack are three times of those in the silica/air stack and ~150 times greater than those in the silica/germanosilicate stack (The fractional bandwidths are 0.74, 0.24, and 0.0042 respectively). From this comparison, a silica/air periodic structure should behave similarly to a silicon/air one.

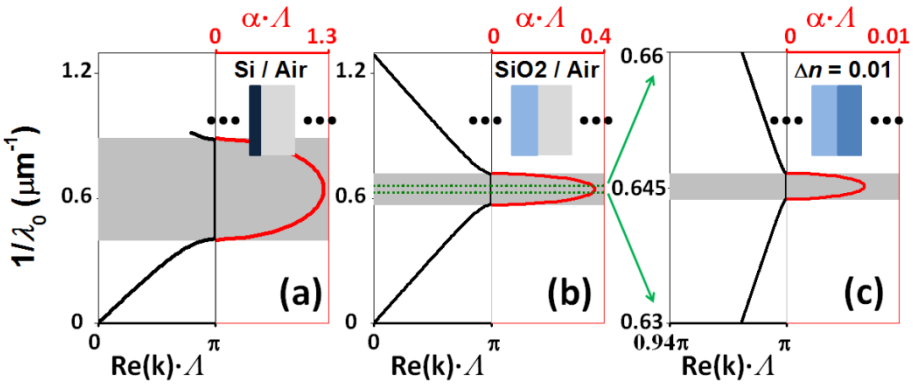


Fig. 1. (Color online) Wave vector diagrams of three quarter-wave stacks: (a) Silicon/air, (b) silica/air, and (c) silica/germanosilica ($\Delta n$=0.01). $\Lambda$ is the period and the scales in the three panels are different.

Figure 2(a) depicts an adiabatically tapered fiber drawn from a conventional single-mode fiber (SMF). The core mode of the SMF on the left is converted to the fundamental mode in the taper waist, and then converted back to the core mode of the SMF on the right with very high efficiency [10], verified by the measured insertion loss less than 0.1 dB. As required by the mode orthogonality, any higher-order mode generated in the taper waist region will be converted to radiation or cladding modes in the SMF which are heavily attenuated at the lossy interface between the silica cladding and the polymer coating [6].

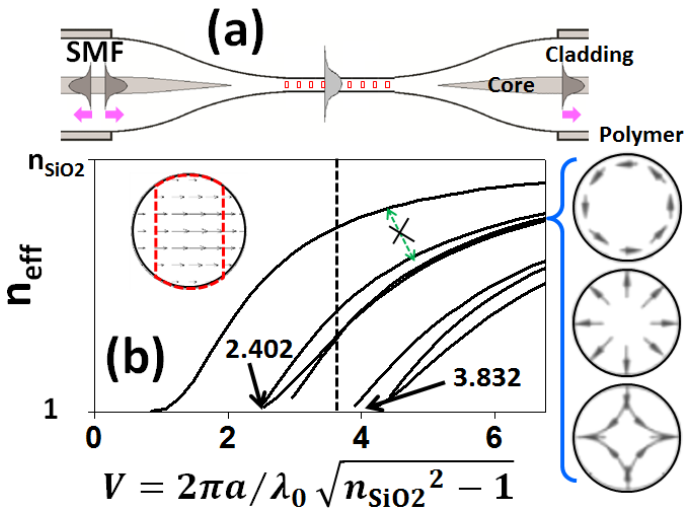


Fig. 2. (Color online) (a) Schematic of an adiabatically tapered fiber and the guided modes therein. (b) Effective modal indexes as a function of the $V$-value of the fiber taper. $2a$ is the taper diameter. Insert: electric field distributions of $HE_{11}$ (left), $TE_{01}$ (right upper), $TM_{01}$ (right middle), and $HE_{21}$ (right lower) modes. The red outlines in (a) and (b) denote the etched holes.

When rectangular holes are drilled through the central region of the fiber taper, the structural symmetry prohibits energy conversion from the fundamental mode ($HE_{11}$) to the first three odd modes ($TE_{01}$, $TM_{01}$, $HE_{21}$). This relaxes the usual condition for single-mode operation ($V < 2.402$) to that for the single-even-mode ($V < 3.832$) [11], allowing us to use somewhat thicker and stronger tapers. A thicker microfiber also mitigates against any contamination-induced device degradation. In this work, we fix the diameter of the microfiber to be ~1.7 μm and the working wavelength to $\lambda_0$ = 1.55 μm [the black dashed line in Fig. 2(b)], where only the fundamental and the first three higher-order guided modes exist, while the latter three guided modes are not excited.

## 3. Experiments and simulations

The lengths of each taper transition and the taper waist are ~20 mm. As shown in Fig. 3(a), nine rectangular holes (1.04×0.16 μm$^2$) are milled along a 1.72 μm-thick section of fiber taper with a period, $\Lambda = 0.63$ μm. The dimensions are determined by scanning electron microscopy. During the milling, a clean silicon wafer serves as a conducting substrate and reduces charging effects. Neither metal nor dielectric coatings [9] are employed to avoid any contamination. The beam spot size and depth of focus of our FIB facility (FEI DB235) are 14 nm and 10 μm respectively. After milling, the fiber taper was detached from the silicon wafer. Although the etched holes occupy 72% of the overall cross section, the microfiber device exhibits surprisingly robust mechanical strength when detached from the substrate.

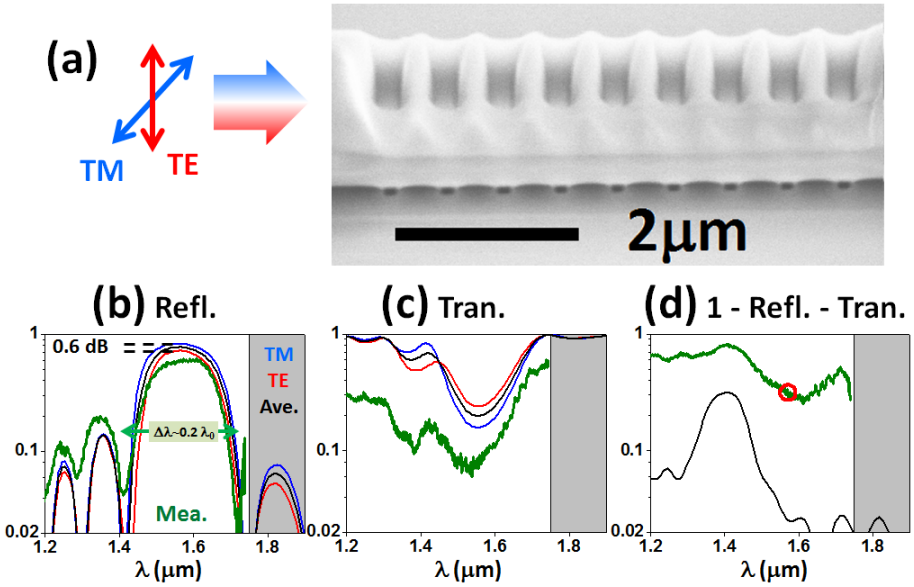


Fig. 3. (Color online) (a) SEM image of a structured microfiber on a Si substrate and schematic indication of the input polarizations. Note that the microfiber has been etched through leaving the visible indentations in the Si substrate. (b-d) Measured (green curve) and simulated (blue/red/ black lines) reflectance, transmittance and loss spectra.

Reflectance and transmittance measurements on the free-standing fiber taper are shown in Figs. 3(b) and 3(c). The measured wavelength range is restricted by the fiber optical circulator and the optical spectrum analyzer in our setup. Supercontinuum light generated in a piece of photonic crystal fiber is used as the source. All the optical components in the measurement setup are in-line fiber devices and are spliced together with very low insertion loss (<0.01 dB) and good repeatability. Since maintaining a single polarization state across a broad wavelength range (1.2-1.75 μm) is difficult in a meter-scale fiber system, the measured spectra should be regarded as the average of TM and TE polarizations, as indicated in Fig. 3(a). Based on the measured geometric parameters and the simulated local modal indices in the unetched/etched taper sections ( $n_{eff}^{(U,E)}$ ), the normalized stop band width (defined in Ref. [12]) of our periodic waveguide is estimated to be greater than 10%, which agrees well with the spectral measurements.

For further comparison, Figs. 3(b) and 3(c) also show finite-difference time-domain (FDTD) simulated results for two polarizations together with their averages. In the simulation, two 1.26 μm diameter microfibers, whose single-even-mode ( $V < 3.832$ ) operation condition covers the wavelength region $\lambda_0$ >1.1 μm, are used as the input and output waveguides. Via two adiabatic transitions, they are connected with a 1.72 μm-diameter microfiber containing an array of perfectly rectangular through-holes. Such a configuration mimics experiment by ensuring that only the fundamental mode ($HE_{11}$) contributes to the spectra. Without these fictitious input and output microfibers, even higher-order modes ($EH_{11}$, $HE_{31}$…) will contribute to the transmittance and reflectance in the simulation. Note that, in the short wavelength region ($\lambda_0$ <1.46 μm), the $HE_{11}$ mode couples to these even-parity higher-order modes in the structured microfiber region, while in experiments these modes are converted to cladding modes in the SMF and are strongly attenuated.

It can be seen that the peak wavelength and the positions of the first-minima on either side in the measured reflectance spectrum agree well with the simulated result in Fig. 3(b). The fractional bandwidth is ~20% which is one order of magnitude greater than previously

reported for a freely-suspended microfiber reflector [8]. The average modal index in the PhC region is $\tilde{N}_{eff} = \lambda_0/(2\Lambda) \approx 1.23$, which is approximately equal to the arithmetic mean of the simulated local modal indices of the unetched ( $n_{eff}^{(U)} = 1.33$ ) and the etched [ $n_{eff}^{(E)} = 1.02$/ 1.06 (TM/TE)] microfiber. The modal index contrast, defined as $(n_{eff}^{(U)} - n_{eff}^{(E)})/n_{eff}^{(U)} = 0.2$, is much greater than that in Ref. [8] ($\Delta n_0/n_0 = 0.01$) and leads to a significantly larger reflection bandwidth. The calculated difference in the peak reflectance in TM and TE polarizations [~0.6 dB comparing the blue and the red lines in Fig. 3(b)] is also close to that observed by monitoring the reflected power at the peak wavelength whilst rotating the paddles of an in-line polarization controller. The only significant discrepancy between measurement and simulation is the lower measured peak reflectance (0.60 compared with 0.77), which may be attributed to non-ideal fabrication.

The measured transmission spectrum in Fig. 3(c) shows a dip at the wavelength $\lambda_0 \approx 1.55$ μm in accord with the simulation, but the transmission at shorter wavelengths is much lower than predicted. As mentioned above, for wavelengths shorter than 1.46 μm coupling between the $HE_{11}$ mode and even-parity higher-order modes becomes important whilst below 1.42 μm the $HE_{11}$ mode starts to couple with the radiation mode because the wavevector of the corresponding Bloch mode falls into the air light cone [13] [see Fig. 4(a)]. Both of these effects will degrade the transmission. However, they have been taken into account in the simulations so that we believe the discrepancy between the measurement and simulation in Fig. 3(c) is due to the loss induced by a small tilt of the inner walls of the etched holes which is an artifact of the ion beam etching. The shape of the hole is trapezoidal, and the estimated angle between two walls is ~ $9^o$. Preliminary tests show that this angle can be reduced by further optimization of the fabrication process.

Figure 4 shows the wave-vector diagrams of our device and that described in Ref. [8] calculated using a commercial plane-wave-expansion band solver. The stop bands (red lines) of these two periodic structures exhibit fractional bandwidths of ~9.3% and ~1.0% respectively. Both lie outside of the air light cones (the gray areas in Fig. 4), which verifies the existence of leakage-free Bloch guided modes. In contrast, the light cone for $n$ ~ 1.373 (the green area) covers the stop band in Fig. 4(a). This corresponds to the situation in Ref. [9] and may explain why the reflected spectrum in that work exhibits unwanted structure since coupling to high order modes in the polymer cladding is then allowed.

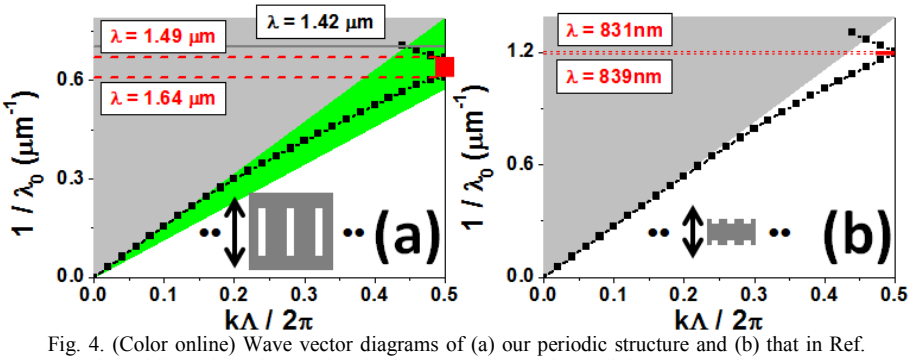


Fig. 4. (Color online) Wave vector diagrams of (a) our periodic structure and (b) that in Ref. [8]. The red lines show the stop bands, the gray areas are the air light cones, and the green area is the light cone for $n$ = 1.373. The double ended arrows in (a) and (b) indicate the polarization axes.

Although exhibiting strong photonic crystal effects, our structured microfiber suffers from radiation loss, as revealed by the non-complementary transmittance and reflectance spectra [Fig. 3(d)]. Apart from the already mentioned loss associated with unintentional

fabrication artifacts there is additional loss associated with the transitions between structured and unstructured fiber, as pointed out in Ref. [14]. Simulations show that although an incident guided wave in the unstructured fiber predominantly couples to the Bloch wave in the PhC waveguide section, changes in effective modal index can give rise to significant coupling to forward-tilted radiation modes at the interface between these two sections. Similar energy coupling to forward-tilted radiation modes also occurs when the Bloch wave leaves the PhC section. In Ref. [15], we analyzed the interference between such radiated waves in a low-index PhC waveguide and pointed out that it can be engineered by adjusting the length of the PhC section in order to couple part of the radiated energy back into the waveguide. We have examined this hypothesis experimentally by constructing a series of microfiber-based PhC reflectors with the same dimensions as above except for different numbers of periods, *N*. Radiation loss at the center of the stop band in each device was estimated from the measured transmittance and reflectance spectra with the result shown in Fig. 5. The undulation in the radiation loss with varying *N* is a signature of interference and the position of the maximum radiation loss at $N = 4$ is very close to that predicted in Ref. [15]. As discussed in more detail in Ref. [15], the radiation mainly comprises three components, denoted as 1, 2 and 3 in the inset of Fig. 5. Waves 1 and 2 are in the same direction and can interfere with each other. They are respectively caused by propagation of the guided wave from a high-index waveguide (the unetched microfiber, $n^{(H)}$) to a low-index waveguide (the PhC microfiber with effective modal index, $n^{(L)}$) and vice-versa. The field coupling coefficient between the incident guided wave and the radiated wave, $C \propto \frac{n_{eff}^{(in)} - n_{eff}^{(out)}}{n_{eff}^{(in)} + n_{eff}^{(out)}}$, has opposite sign for radiated waves 1 and 2 in Fig. 5. Here, $n_{eff}^{(in,out)}$ stands for the effective index of the local mode in the input and the output waveguide, respectively. Thus these waves have a π phase difference at their points of origin to which the phase difference associated with propagation across the region of space containing the PhC must be added. The net phase difference between waves 1 and 2 is then equal to $\frac{\pi}{\Lambda} \cdot N\Lambda - \frac{2\pi}{\lambda_0} \cos\theta \cdot N\Lambda + \pi$. The first term is the phase difference associated with propagation of the guided Bloch wave across the PhC waveguide section. The second term is associated with propagation of wave 1 in air. The exact value of the tilt angle $\theta \approx 15^{\circ}$ has only a small effect on the result. Using the values $\Lambda = 0.63\mu m$ and $\lambda_0 = 1.55\mu m$, we obtain constructive (destructive) interference and radiation loss maximum (minimum) near $N = 4(6)$.

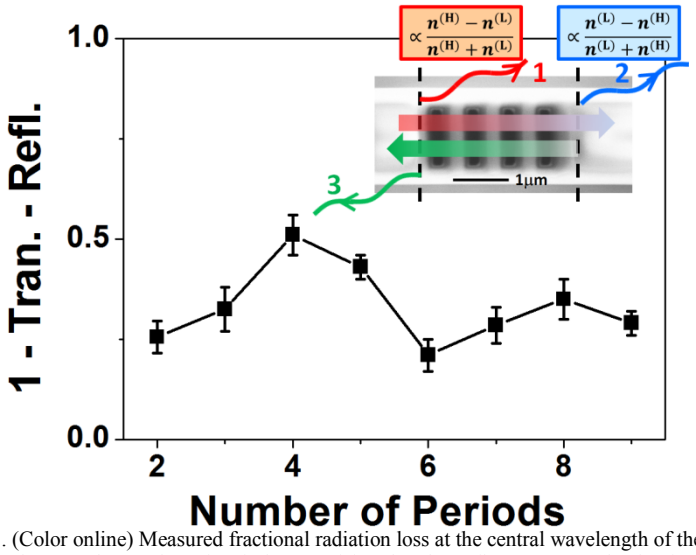


Fig. 5. (Color online) Measured fractional radiation loss at the central wavelength of the stop band versus the number of periods comprising the PhC reflector. Insert: the dominant contributions to the scattering loss at the transitions are labeled 1 to 3.

## 4. Conclusions

In conclusion, a PhC reflector with a fractional reflection bandwidth in excess of 10% and a device length of only a few wavelengths has been fabricated in a silica microfiber. The measured transmittance and reflectance spectra agree well with simulation when allowing for the complexities introduced by the inclined inner walls of the etched holes. We have quantified the radiation loss at the center of the stop band and explain its variation with the number of periods as due to interference. Although the loss at the center of the stop band is presently high (~30%), simulations suggest that this could be reduced by an order of magnitude if the fabrication process can be improved. By drilling holes through the core of a microfiber taper and adopting single-even-mode propagation condition, rather than the usual single-mode condition, we simultaneously obtain a strong photonic crystal effect and robust, freely-suspended operation which may inspire future applications in nano-photonics.


### Acknowledgements

We thank Ai-zi Jin for help with fabrication. This work was supported by the National Basic Research Foundation of China (No. 2011CB922002), the National Natural Science Foundation of China (No. 61275044 & No. 11204366), and the 100 Talents Programme of the Chinese Academy of Sciences (No. Y1K501DL11).